

Genome analysis

# Multiresolution correction of GC bias and application to identification of copy number alterations

Ho Jang and Hyunju Lee\*

School of Electrical Engineering and Computer Science, Gwangju Institute of Science and Technology, Gwangju 500-712, South Korea

\*To whom correspondence should be addressed.

Associate Editor: Inanc Birol

Received on May 24, 2018; revised on March 3, 2019; editorial decision on March 7, 2019; accepted on March 12, 2019

## Abstract

**Motivation:** Whole-genome sequencing (WGS) data are affected by various sequencing biases such as GC bias and mappability bias. These biases degrade performance on detection of genetic variations such as copy number alterations. The existing methods use a relation between the GC proportion and depth of coverage (DOC) of markers by means of regression models. Nonetheless, severity of the GC bias varies from sample to sample. We developed a new method for correction of GC bias on the basis of multiresolution analysis. We used a translation-invariant wavelet transform to decompose biased raw signals into high- and low-frequency coefficients. Then, we modeled the relation between GC proportion and DOC of the genomic regions and constructed new control DOC signals that reflect the GC bias. The control DOC signals are used for normalizing genomic sequences by correcting the GC bias.

**Results:** When we applied our method to simulated sequencing data with various degrees of GC bias, our method showed more robust performance on correcting the GC bias than the other methods did. We also applied our method to real-world cancer sequencing datasets and successfully identified cancer-related focal alterations even when cancer genomes were not normalized to normal control samples. In conclusion, our method can be employed for WGS data with different degrees of GC bias.

**Availability and implementation:** The code is available at <http://gcancer.org/wabico>.

**Contact:** [hyunjulee@gist.ac.kr](mailto:hyunjulee@gist.ac.kr)

**Supplementary information:** [Supplementary data](#) are available at *Bioinformatics* online.

## 1 Introduction

The whole-genome sequencing (WGS) technology is widely used for identifying innate or acquired genetic variations. Nevertheless, the quality of WGS data can be affected by various sequencing biases such as GC bias and mappability bias. These biases affect performance on detection of genetic variations such as copy number (CN) alterations. In case of a cancer study, paired normal control sequencing data can serve for correcting these biases (Teo *et al.*, 2012). Nonetheless, both tumor and normal control sequencing data should be generated under the same conditions. Another popular

method is to adjust the observed depth of coverage (DOC) of a specific genomic window on the basis of the GC proportion of the window (Magi *et al.*, 2012), as shown in the following formula:

$$DOC_{i,corrected} = DOC_{i,raw} \cdot \frac{DOC_{average}}{DOC_{i,GC}}, \quad (1)$$

where  $DOC_{i,raw}$  is the DOC of specific window  $i$ ,  $DOC_{average}$  is the average DOC of all genomic windows and  $DOC_{i,GC}$  is the value of DOC reflecting the level of GC bias of window  $i$ . The simplest estimation for  $DOC_{i,GC}$  is to calculate the average DOC of the genomic

windows with the same GC proportion as that of window  $i$ . The relation between GC proportion and DOCs  $DOC_{i,GC}$  can be modeled by means of regression models such as LOESS regression (Scheinin *et al.*, 2014) or polynomial regression (Boeva *et al.*, 2011). Some studies (Benjamini and Speed, 2012; Xi *et al.*, 2016) model the GC bias via the number of reads mapped to the genomic position at a nucleotide level rather than the genomic window level. On the other hand, there are no widely accepted methods for modeling GC bias in the DOC signal because the severity of GC bias varies sample to sample, and factors that cause GC bias are not yet fully identified.

In this study, we developed a new GC bias correction method based on multiresolution bias correction named Wabico (WAvelet transform-based Bias COrrrection). We used a translation-invariant (TI) wavelet transform (Coifman and Donoho, 1995) to decompose GC-biased original DOC signals. Then, we modeled the relation between GC proportions and DOC of the genomic regions and constructed artificial control DOC,  $DOC_{GC}$ , which reflects GC bias. When we investigated the performance of our proposed method on GC bias correction in simulated sequencing data and real cancer WGS data, Wabico showed better performance in samples with severe bias than the other methods did.

## 2 Materials and methods

Figure 1 shows the procedure of the Wabico method. For a WGS Binary Alignment Map (BAM) file, the mapped reads within genomic windows are counted. These windows consist of the same number of uniquely mappable positions (Fig. 1a). We decompose the DOC signal of the genomic windows using the TI wavelet transform (Fig. 1b). It produces scaling coefficients and wavelet coefficients. The scaling coefficients represent the average of DOC values between two neighboring regions, and the relation between scaling coefficients and their GC proportion is modeled by LOESS regression (Fig. 1c). The wavelet coefficients denote the difference in DOC values between two neighboring genomic regions, and the relation between the wavelet coefficients and their GC proportions is modeled by two-dimensional (2D) kernel smoothing (Fig. 1d). After fitted coefficients are obtained,  $DOC_{GC}$  values are generated that represent the GC bias embedded in input WGS data (Fig. 1e). These  $DOC_{GC}$  values are used for correcting GC bias at each decomposition level. By checking the criterion based on the amount of direction of changes consistent with the initial direction of GC changes, we determine whether the decomposition stops or not (Fig. 1f). If further decomposition is necessary to take into account broader genomic regions of the DOC values, the current scaling coefficients will be decomposed into a higher level of scaling coefficients and wavelet coefficients. The steps from (b) to (f) are repeated until the stopping criterion is satisfied. Each step will be explained in more detail. Finally,  $DOC_{GC}$  values generated at the highest level that meet the stopping criteria are suggested to correct the GC bias of the raw DOC values.

### 2.1 CN quantification

The input of Wabico is DOC values obtained from WGS data. DOC is the number of mapped sequencing reads within a given genomic region. In early studies, the size of the genomic region for measuring DOC was fixed (Teo *et al.*, 2012). After that, BIC-Seq2 (Xi *et al.*, 2016) started to use variable-size genomic windows by taking into account the mappability of the sequencing reads. As in BIC-Seq2, we employed variable-size windows containing equal numbers of uniquely mappable positions.

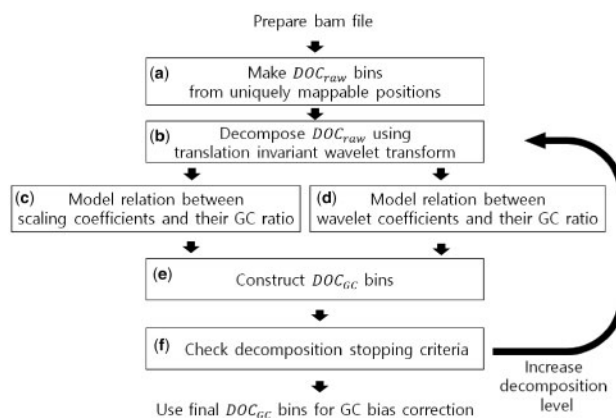


Fig. 1. An overview of GC bias correction steps

### 2.2 Decomposition of DOC values via the TI wavelet transform

Raw DOC values are decomposed into wavelet and scaling coefficients using the TI wavelet transform (Coifman and Donoho, 1995) with the Harr wavelet. We chose the TI wavelet transform because it shows better signal recovery performance as compared to the usual discrete wavelet transform (Coifman and Donoho, 1995). At every decomposition level, it utilizes both the given signal and the circularly shifted signal to the right. Figure 2(a–c) shows an example of DOC signal decomposition up to level 2, where the input DOC signal consists of 32 windows. Figure 2(a–c) illustrates the changes of a TI-Table, which is a data structure used in the TI wavelet transform. Given a raw DOC signal [(1) in Fig. 2], it is decomposed into scaling coefficients and wavelet coefficients [(2) and (3) in Fig. 2]. The size of the two resulting coefficients is 16, i.e. a half of the input signal. For maintaining the translation invariance property, a shifted version of the input DOC signal is also decomposed into scaling coefficients and wavelet coefficients [(4) and (5) in Fig. 2]. The scaling coefficients of current level 1 [(2) and (4) in Fig. 2] can be decomposed further into a higher level of scaling coefficients and wavelet coefficients. Figure 2(c) shows the results of decomposition from the TI-Table presented in Figure 2(b). Scaling coefficients (6) and wavelet coefficients (7) come from scaling coefficient (2). Scaling coefficients (8) and wavelet coefficients (9) come from the shifted version of scaling coefficient (2). The sizes of coefficients (6), (7), (8) and (9) are all 8 and a half of the size of coefficient (2) at the previous level 1. Similarly, coefficients (10), (11), (12) and (13) of level 2 come from scaling coefficient (4). In summary, the scaling coefficients of the current level can be decomposed into scaling coefficients and wavelet coefficients of the next level. The detailed procedure is described in the article about the TI wavelet transform (Coifman and Donoho, 1995).

### 2.3 Modeling the relation between scaling coefficients and their GC proportion

After scaling and wavelet coefficients for all given chromosomes are calculated, the relations between these coefficients and their GC proportion are modeled. First, GC proportions for these coefficients are calculated. The scaling coefficient of level 1 covers twice the genomic areas covered by the input signal of level 0. In addition, the scaling coefficient of level  $j$  covers twice the genomic areas covered by the scaling coefficient of level  $j - 1$ . Every scaling coefficient has its own corresponding GC proportion. The GC proportion of the scaling coefficient for level  $j$  is  $GC_{j,i} = GC_{j-1,2i-1} + GC_{j-1,2i}$ , where

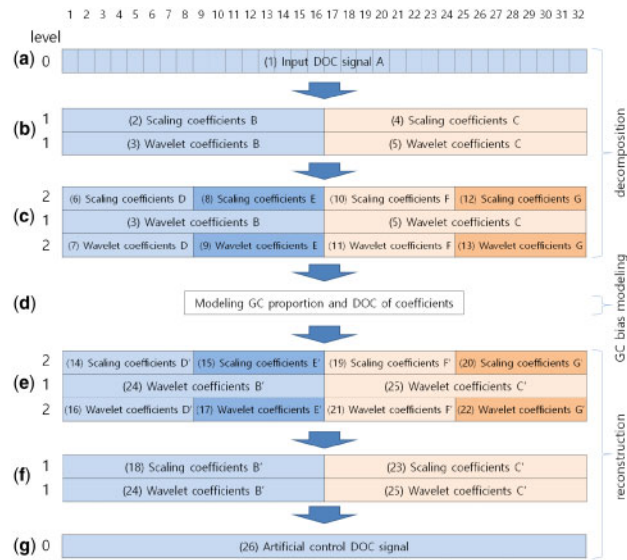


**Fig. 2.** An example of TI-Tables during raw DOC signal decomposition and construction of an artificial control DOC signal. (a) A TI-Table of the input DOC signal consisting of 32 windows. It is a  $1 \times 32$  numerical matrix. (b) The TI-Table after signal decomposition from the input DOC signal (a). This is a  $2 \times 32$  matrix. (c) The TI-Table after signal decomposition of scaling coefficients from (b). TI-Table size is  $3 \times 32$ . (d) The modeling step for these coefficients. (e) The TI-Table consisting of fitted coefficients from the previous modeling step. (f) The TI-Table after averaging out of the scaling coefficient and the wavelet coefficient of level 2 in TI-Table (e). (g) The TI-Table containing an artificial control DOC signal after averaging out of the coefficients of TI-Table (f)

$i$  is the index of the coefficient of level  $j$ . The GC proportion for the shifted scaling coefficient is  $GC_{j,i} = GC'_{j-1,2i-1} + GC'_{j-1,2i}$ , where  $GC'_{j-1}$  is the shifted version of  $GC_{j-1}$ . [Supplementary Figure S1](#) shows an example of GC proportion calculation.

Given all pairs of GC proportion and a scaling coefficient from given chromosomes for level  $j$ , LOESS regression (Cleveland, 1979) is used for fitting relation  $coef_{scaling,j} = loess(GC_j)$ . The fitted  $coef_{scaling,j}$  is employed for constructing  $DOC_{GC}$ . The R package limma (Ritchie et al., 2015) provides fast LOESS regression. [Figure 3\(a\)](#) depicts a distribution of raw scaling coefficients and their GC proportions at decomposition level 6 of the simulated data generated by Pysim-sv (Xia et al., 2017) with GC biases at  $z = 30$ . The details of the simulated sequence generation will be explained in Section 3. The red curve represents the LOESS-fitted scaling coefficients.

## 2.4 Modeling the relation between wavelet coefficients and their GC proportion

Wavelet coefficients denote the DOC differences between two neighboring genomic regions in the reference sequence. Because of the difference in GC proportions between the two neighboring genomic regions, a DOC difference between the genomic regions may occur. To construct  $DOC_{GC}$ , the DOC difference should be modeled by means of the GC proportion of the two adjacent regions. The GC proportions of the wavelet coefficients for level  $j$  are  $GC_{left,j,i} = GC_{j-1,2i-1}$  and  $GC_{right,j,i} = GC_{j-1,2i}$ , where  $i$  is the index of the coefficient of level  $j$ . The GC proportions of the wavelet coefficients for the shifted scaling coefficient of previous level  $j-1$  are  $GC'_{left,j,i} = GC'_{j-1,2i-1}$  and  $GC'_{right,j,i} = GC'_{j-1,2i}$ , where  $GC'_{j-1}$  is the shifted version of  $GC_{j-1}$ . [Supplementary Figure S1](#) shows an example of GC proportion calculation.

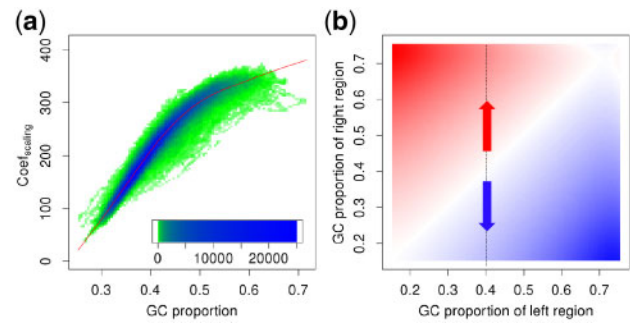


**Fig. 3.** The relation between coefficients and their GC proportions for the simulated GC-biased sequencing reads. (a) The relation between GC proportion and a scaling coefficient. The heatmap represents the distribution of raw scaling coefficients. The x-axis means the GC proportion of the coefficients, and the y-axis denotes the value of the coefficients. Most of scaling coefficients are concentrated in blue areas. The scaling coefficients are rarely distributed in the green areas. The red curve is the LOESS-fitted scaling coefficient depending on the specific GC proportion. (b) The relation between two neighboring GC proportions and a wavelet coefficient. The heatmap indicates the relation between the value of wavelet coefficients (pixel color) and the GC proportion of two neighboring genomic regions (x-axis and y-axis) from 2D kernel smoothing. Red areas represent the increasing DOC values of the right-hand genomic region compared to the left-hand region in the two adjacent genomic regions. The blue areas mean the opposite case

For all the given wavelet coefficients at level  $j$ , the relation  $coef_{wavelet,j} = smoother(GC_{right,j}, GC_{left,j})$  is modeled, where  $coef_{wavelet,j}$  is a wavelet coefficient for two adjacent GC proportions  $GC_{right,j}$  and  $GC_{left,j}$  at level  $j$ . We used an approximate Nadaraya Watson kernel smoother provided by the smooth.2d function of the R field package (Douglas et al., 2015).

[Figure 3\(b\)](#) shows the smoothed results representing the relation between GC proportions of consecutive genomic regions and wavelet coefficients at decomposition level 6 of the simulated data generated by Pysim-sv (Xia et al., 2017) with GC biases at  $z = 30$ . The x-axis represents the GC proportion of the left-hand genomic region, the y-axis represents the GC proportion of the right-hand genomic region and the color represents the value of wavelet coefficients. In this figure, when GC proportion of the left-hand region is 0.4 and the GC proportion of the right-hand region is greater than 0.4, the value of the wavelet coefficient between the two neighboring regions is positive (red pixel), and the DOC increases. On the other hand, if GC proportion of the left-hand region is 0.4 and the GC proportion of the right-hand region is less than 0.4, the value of the wavelet coefficient between the two neighboring regions is negative (blue pixel), and the DOC decreases. [Supplementary Figure S2](#) illustrates another example of a relation between coefficients and their GC proportion.

## 2.5 Construction of $DOC_{GC}$

After obtaining fitted scaling coefficients from LOESS regression and smoothed wavelet coefficients from kernel smoothing, we construct the  $DOC_{GC}$  that represents the GC bias embedded in the raw input DOC signal. We prepare an empty TI-Table data structure. Each element of the TI-Table matches genomic regions that have GC proportion information as we mentioned in the previous sections. We can set the value of every element in the TI-Table to the fitted coefficients calculated at the previous steps because these values have their own GC proportion information. After we fill in all the values of the TI-Table, the  $DOC_{GC}$  is constructed by means of the TI wavelet inverse transform.

For example, Figure 2(e–g) shows an example of construction of  $DOC_{GC}$ . Scaling coefficients (14) of level 2 are up-sampled. Scaling coefficients (15) are up-sampled and then shifted to the left. These two signals are averaged for maintaining the translation invariance property. Similarly, wavelet coefficient (16) is up-sampled. Wavelet coefficient (17) is up-sampled and then shifted to the left. These two signals are also averaged for the same reason. Scaling coefficient (18) for level 1 is generated by summing these two averaged signals. Scaling coefficient (23) is calculated from coefficients (19), (20), (21) and (22) in the same way as in the construction of coefficient (18). Besides, artificial control DOC signal (26),  $DOC_{GC}$ , is generated from coefficients (18), (23), (24) and (25) in the same way. The details of this TI wavelet inverse transform are described by Coifman and Donoho (1995).

After that, GC bias-corrected CNs are calculated via the following formula:

$$CN_{i,Wabico} = \frac{DOC_{i,raw}}{DOC_{i,GC}}, \quad (2)$$

where  $DOC_{i,raw}$  is the raw DOC of specific window  $i$ ,  $DOC_{i,GC}$  is  $DOC_{GC}$  of windows  $i$ .  $DOC_{GC}$  serves to control GC bias and to normalize the DOC signal. If  $CN_i$  is close to 1.0, then the CN of genomic window  $i$  is close to ploidy of chromosomes in the cell.

## 2.6 The boundary problem

The input signal length in the TI wavelet transform should be  $2^l$ . Because the genomic lengths of chromosomes are not usually  $2^l$ , the signal should be modified accordingly. Given DOC signals or CN ratio signals, we create a new input signal of length  $2^l$  by extending the original signal symmetrically and periodically. The boundary problem was handled in a study by Hur and Lee (2011).

## 2.7 Determination of the decomposition level

The amount of GC bias varies from sample to sample. Although some samples can be corrected using  $DOC_{GC}$  constructed from the low decomposition levels, if samples are severely affected by GC bias, the  $DOC_{GC}$  constructed at higher decomposition levels may be more effective. To adaptively correct GC bias,  $DOC_{GC}$  signals constructed from the low decomposition level to the high decomposition level are sequentially applied to the raw DOC signals to calculate  $CN_{Wabico}$  values. In addition, we developed a criterion for determining a proper decomposition level.

When levels change from  $i$  to  $i+1$ , for each GC window, the  $CN_{Wabico}$  value at level  $i$  is compared with that at level  $i+1$ , and the direction of change of  $CN_{Wabico}$  is determined: an increase in  $CN_{Wabico}$  or a decrease in  $CN_{Wabico}$ . Directions of changes in  $CN_{Wabico}$  from level 1 to level 2 across all GC windows are referred to as the initial direction of changes, and they are employed to check the consistency of direction of the changes for further level decomposition. The proper decomposition level for the WGS data is determined by the ratio of consistency values between the direction of changes at a given level and the initial direction of changes.

Figure 4 shows an example of the sequential GC corrections and determination of a proper decomposition level for the simulated sequencing data. Initially,  $CN_{Wabico}$  values corrected by means of  $DOC_{GC}$  from decomposition level 1 are calculated [gray line in Fig. 4(a)]. Next, the GC bias in the raw DOC signal is corrected using  $DOC_{GC}$  from decomposition level 2 [black line in Fig. 4(a)]. The curve of  $CN_{Wabico}$  at level 2 is closer to the value 1.0 on the y-axis than that of  $CN_{Wabico}$  at level 1. The y-axis value 1.0 represents an even distribution of CN values regardless of GC proportion in

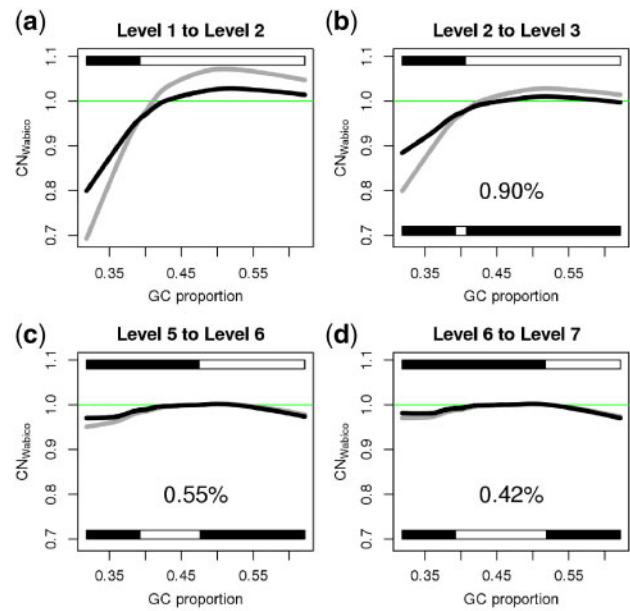


**Fig. 4.** An example of multiresolution GC bias correction. (a)  $CN_{Wabico}$  values from level 1 (gray) to level 2 (black). (b)  $CN_{Wabico}$  values from level 2 (gray) to level 3 (black). (c)  $CN_{Wabico}$  values from level 5 (gray) to level 6 (black). (d)  $CN_{Wabico}$  values from level 6 (gray) to level 7 (black). Upper bars in all the panels show the direction of changes from level  $i$  to level  $i+1$ . The black color and white color in these upper bars indicate increasing and decreasing directions, respectively. Bottom bars in panels (b), (c) and (d) denote the ratio of change directions consistent with the initial direction of changes. Black areas represent the proportion consistent with the initial direction of changes.  $CN_{Wabico}$  values on the y-axis are the average of  $CN_{Wabico}$  at 102 400 uniquely mappable positions

the genomic windows. Here, the direction of changes in  $CN_{Wabico}$  is increasing in genomic windows whose GC proportion is less than 0.4 [white color in the bar of Fig. 4(a)], while that of  $CN_{Wabico}$  is decreasing in genomic windows whose GC proportion is greater than 0.4 [black color in the bar of Fig. 4(a)]. These directions of changes from level 1 to level 2 for all GC windows are the initial directions of changes. Figure 4(b) presents  $CN_{Wabico}$  values corrected with  $DOC_{GC}$  from level 2 (gray curve) to level 3 (black curve). The black color in the bottom bar of Figure 4(b) denotes the GC proportions in which directions of changes are consistent with the initial direction of changes from level 1 to level 2, showing that 90% of the GC proportions are consistent. We continue to decompose until the consistent proportion is less than 50%. Figure 4(d) indicates that the consistent proportion is less than 50% when the decomposition level is greater than 6. Thus,  $DOC_{GC}$  from the level 6 decomposition is finally selected for correcting GC bias in the raw DOC signal [Fig. 4(c)]. Details about the decomposition stopping criteria are provided in Supplementary Figure S3, Figure S4 and Section 1.4.

## 2.8 GC bias correction by other methods

We compared the performance of Wabico with that of the following approaches to GC bias correction. The uncorrected CN ratio signal is calculated using the following formula:

$$CN_{i,raw} = \frac{DOC_{i,raw}}{\text{median}(DOC_{k,raw})}, \quad (3)$$

where  $\text{median}(DOC_{k,raw})$  is the median of all raw DOCs from the given chromosomes.

In the naive GC correction method, the corrected CN ratio signal is calculated from the GC proportion of the fixed window with a size of 100 bp. It is computed via the following formula:

$$CN_{i,naive} = \frac{DOC_{i,raw}}{\text{mean}(DOC_{GC(k)=GC(i),raw})}, \quad (4)$$

where  $\text{mean}(DOC_{GC(k)=GC(i),raw})$  is the average of  $DOC_{raw}$  bins whose GC value is equal to the GC of the  $i$ th bin.

The corrected CN ratio signal from the BIC-Seq2-based expected read count is calculated by means of the following formula:

$$CN_{i,BIC-Seq2} = \frac{DOC_{i,raw}}{DOC_{i,expected}}, \quad (5)$$

where  $DOC_{i,expected}$  is the expected numbers of reads in bin  $i$  generated from the BIC-Seq2 normalization step.

### 3 Results

We applied Wabico to the simulated sequencing reads containing GC bias. We also applied Wabico to the real glioblastoma multi-forme (GBM), ovarian cancer (OVC) and lung adenocarcinoma (LUAD) WGS datasets from TCGA. Authorization was obtained from the database of Genotypes and Phenotypes (accession No. phs000178.v8.p7). The real data were generated on the Illumina HiSeq or GenomeAnalyzer platform. All the BAM files are aligned to the hg19 human reference sequence.

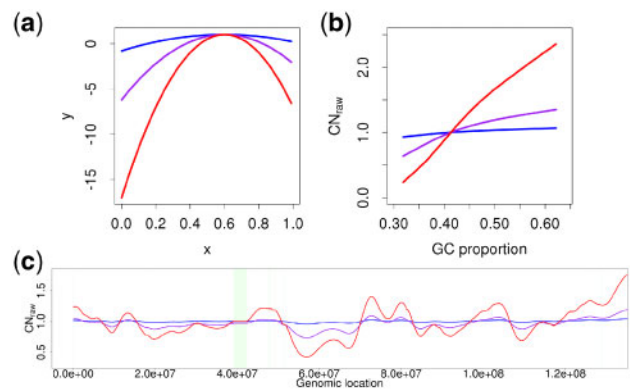
For quantifying DOC values of the WGS data, we set a genomic window consisting of 100 uniquely mappable genomic positions, where a 50mer sequence at the position is uniquely aligned to that position but not elsewhere (Xi *et al.*, 2016). In this section, we denoised the CN signals by a TI wavelet transform denoising procedure (Coifman and Donoho, 1995) before investigating GC effects in the CN signals. To get denoised CN signals, we decomposed a CN signal up to decomposition level 15 and set the wavelet denoising parameter  $C$  to 2. See Jang *et al.* (2016) for details of the denoising procedure.

#### 3.1 GC bias correction in simulated data

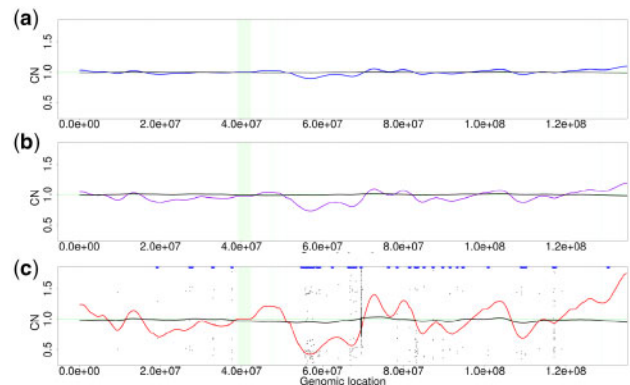
We used Pysim-sv (Xia *et al.*, 2017) for generating simulated short sequencing reads. Chromosomes 8 and 22 from hg19 were selected for the simulation. First, we created diploid sequences of chromosomes 8 and 22 and then generated 100 bp short reads with  $30\times$  coverage. Because Pysim-sv has a function for simulating GC bias, we generated various patterns of GC biases based on the formula  $y = -z \times (x - 0.6)^2 + 1$  in Pysim-sv, where  $x$  represents the GC proportion of the sequencing reads,  $y$  denotes a sampling rate and  $z$  is a constant value: 2.5 in the original code. Severity of the GC bias increases as  $z$  increases. Figure 5(a) presents the results on three  $z$  values such as 5 (blue), 20 (purple) and 50 (red). Figure 5(b) shows LOESS-fitted GC bias curves of  $CN_{raw}$  from the sequencing reads for these  $z$  values. Figure 5(c) depicts a  $CN_{raw}$  signal representing fluctuations of GC bias for three  $z$  values. As  $z$  increases, the fluctuation of the signal increases.

Figure 6(a, b and c) shows the results of GC bias correction by Wabico for simulated reads with  $z$  values of 5, 20 and 50, respectively. Black lines in the plots represent  $CN_{Wabico}$  values. Readers can see that even if GC biases increase severely, the fluctuations of  $CN_{Wabico}$  values decrease effectively.

We compared other approaches with Wabico:  $CN_{BIC-Seq2}$ ,  $CN_{naive}$  and  $CN_{raw}$ . Because the standard deviations (SD) of CN values after GC correction decrease as GC is corrected better, we



**Fig. 5.** GC bias effects from simulated sequencing reads for various  $z$  values. (a) Plots for the GC bias formula at  $z$  values of 5 (blue), 20 (purple) and 50 (red), where the  $x$ -axis and  $y$ -axis represent the  $x$  and  $y$  values in  $y = -z \times (x - 0.6)^2 + 1$  in Pysim-sv, respectively. (b) LOESS-fitted GC bias curves of  $CN_{raw}$  for the three  $z$  values.  $CN_{raw}$  values on the  $y$ -axis are the average of  $CN_{raw}$  at 102 400 uniquely mappable positions. (c)  $CN_{raw}$  at various  $z$  values. The green area represents the centromere region of the chromosome in the reference sequence



**Fig. 6.** CNs corrected by Wabico. The blue signal in panel (a), the purple signal in (b) and the red signal in (c) are the same signals  $CN_{raw}$  with the corresponding colors in Figure 5 (c). The black signals in (a), (b) and (c) are  $CN_{Wabico}$  for Wabico

compared SDs of CN ratios among these four approaches. In Figure 7, blue, green, red and black lines are SDs of  $CN_{raw}$ ,  $CN_{naive}$ ,  $CN_{BIC-Seq2}$  and  $CN_{Wabico}$  at various  $z$  values. SDs of  $CN_{Wabico}$  values are smaller than those of  $CN_{raw}$ ,  $CN_{naive}$  and  $CN_{BIC-Seq2}$  across various  $z$  values, suggesting that Wabico shows more stable correction performance as compared to the other methods. Supplementary Figure S5 presents the comparison of  $CN_{Wabico}$  and  $CN_{BIC-Seq2}$  when  $z$  is 50.  $CN_{Wabico}$  yields smoother results than  $CN_{BIC-Seq2}$  does. Moreover, we compared the performance of the GC correction methods using the simulated data with CN alterations. We created other simulation data with various levels of GC bias and 10 CN variations that are evenly spaced. CN alterations were identified after GC bias correction by Wabico and BIC-seq2-based expected read count. F1 scores of  $CN_{Wabico}$  were consistently higher than those of  $CN_{BIC-Seq2}$  at any GC bias severity. Details are shown in Supplementary Figure S6.

In addition, we applied Wabico and BIC-Seq2-based expected read count to the WGS data of paired normal samples of the 37 patients with GBM. When SDs of  $CN_{Wabico}$  and  $CN_{BIC-Seq2}$  were compared, SDs of  $CN_{Wabico}$  were smaller in 35 samples (Supplementary Table S1).

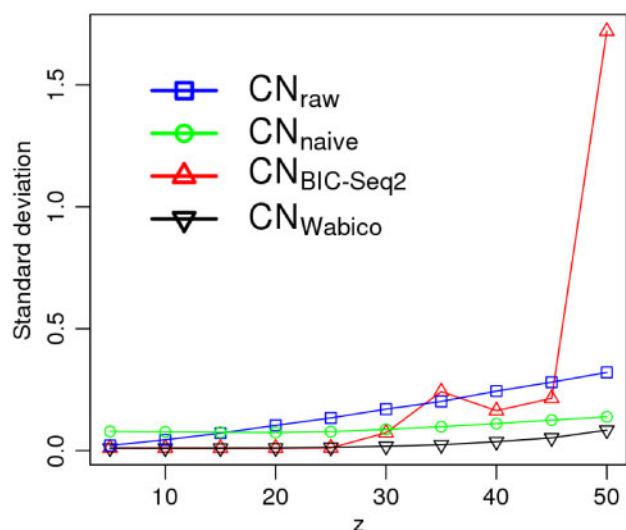


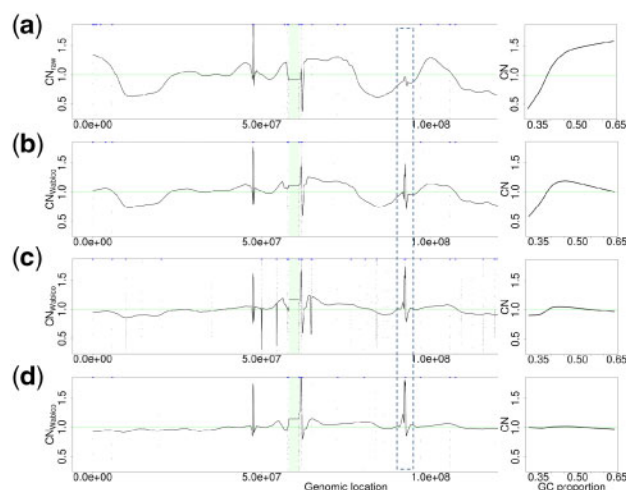
**Fig. 7.** SD of simulated CN ratios at various  $z$  values from 5 to 50. Blue, green, red and black lines represent the SDs of denoised  $CN_{raw}$ ,  $CN_{naive}$ ,  $CN_{BIC-Seq2}$  and  $CN_{Wabico}$  signals, respectively

### 3.2 GC bias correction of real cancer datasets

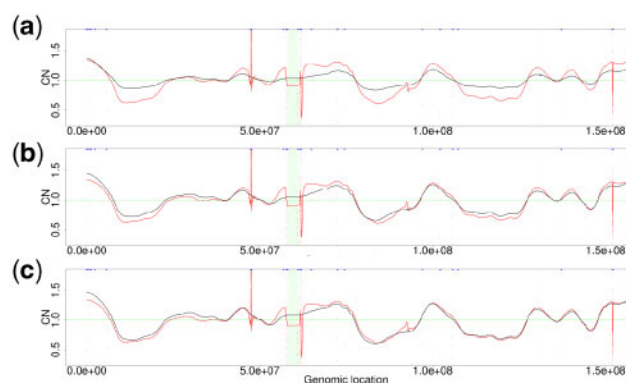
Figure 8 shows the results of GC bias correction via multilevel decomposition of chromosome 7 of the TCGA-15-1444-01A sample from GBM. Left-hand plots of Figure 8 depict the denoised CN values, and right-hand plots are GC bias curves of the CN ratio in the 102 400 bp of uniquely mappable genomic positions. Genomic regions within the dotted box indicate the CN alterations around *CDK6*, which is known as a gene associated with cancer. Figure 8(a) presents  $CN_{raw}$ , and the alteration around *CDK6* is not distinguished well from the neighboring signals. In addition, due to the severe fluctuation of the signal across chromosome 7, it incorrectly seems that there are severe CN changes across the chromosome. Figure 8(b) shows the effect of GC correction when  $CN_{Wabico}$  values are obtained by GC bias correction at decomposition level 1. The alteration around *CDK6* is more distinguishable than that in Figure 8(a). Although the amplitude of fluctuations decreased, the GC bias still influences the signal. Figure 8(c and d) depicts the results of GC bias correction at decomposition levels 5 and 10. As the decomposition levels increase, the fluctuations decrease significantly and the alterations around *CDK6* are more distinguishable.

Figure 9 illustrates how well the GC bias effect embedded in sample TCGA-15-1444-01A is recovered by the fitted coefficients of TI wavelet transform decomposition. In Figure 9(a–c), the denoised  $CN_{raw}$  (red color) is compared with  $CN_{control} = \frac{DOC_{i,GC}}{\text{median}(DOC_{k,GC})}$  at decomposition levels 1, 5 and 10 (black color), respectively. As decomposition levels increase, the fluctuation patterns of  $CN_{control}$  become more similar to those of  $CN_{raw}$ . Supplementary Figure S7 shows the distribution of  $CN_{Wabico}$ . As decomposition levels increase, the peaks in the distribution become more distinguishable.

In our previous study (Jang et al., 2016), we successfully identified focal alterations around known cancer genes in TCGA WGS data after normalizing tumor samples to paired normal samples. In the present study, we tested whether the alterations around these genes can be identified without normal controls if we apply the proposed GC correction method to tumor samples. A cancer gene was considered to be identified if the two conditions in Supplementary Material were satisfied. Tables 1, 2 and 3 list the known cancer genes and the number of samples with alteration in these genes for GBM, LUAD and OVC WGS datasets, respectively. Wabico



**Fig. 8.** CN signals on chromosome 7 (left) and GC bias curves (right) of sample TCGA-15-1444-01A.  $CN_{Wabico}$  values on the y-axis of the GC bias plots are the average of  $CN_{Wabico}$  at 102 400 uniquely mappable positions. (a)  $CN_{raw}$  values and their GC bias curve. (b)  $CN_{Wabico}$  values and their GC bias curve obtained with  $DOC_{GC}$  constructed from level 1 decomposition. (c)  $CN_{Wabico}$  values and their GC bias curve obtained by means of  $DOC_{GC}$  constructed from level 5 decomposition. (d)  $CN_{Wabico}$  from level 10 decomposition



**Fig. 9.** Similarities of the GC bias pattern between the  $CN_{raw}$  signal and  $CN_{control}$  signal on chromosome 7 of the TCGA-15-1444-01A sample. The red signals in panels (a), (b) and (c) are  $CN_{raw}$  signals in Figure 8(a). The black signals in (a), (b) and (c) are  $CN_{control}$  signals generated at levels 1, 5 and 10, respectively

identified altered cancer genes in most of TCGA samples without normal control data, except for some genes located in regions that are not sufficiently distinguishable as focal aberrations, such as *EGFR* in the TCGA-06-0686-01A GBM sample and *CDK4* in the TCGA-15-1444-01A GBM sample.

In addition, we compared GC bias correction by BIC-Seq2-based expected read counts and by Wabico for identification of these known cancer genes with focal aberrations. For this task, we applied these two GC bias correction methods to tumor samples and then segmented them by the BIC-Seq2 segmentation method. The comparison details and results are presented in Supplementary Tables S2, S3 and S4, showing that Wabico outperformed BIC-Seq2-based expected read counts on GBM, but the two methods identified the same number of genes in LUAD and OVC.

### 3.3 Correlation with SNP array level 3 datasets

We compared  $CN_{Wabico}$  and  $CN_{BIC-Seq2}$  by calculating correlation coefficients between each of them and the CN ratio from SNP array

**Table 1.** CN-altered GBM-related genes

| Chr | Start     | End       | Name   | Type | Total | Identified | Ratio |
|-----|-----------|-----------|--------|------|-------|------------|-------|
| 1   | 204485511 | 204542871 | MDM4   | amp  | 6     | 6          | 1.00  |
| 4   | 1795034   | 1810599   | FGFR3  | amp  | 4     | 4          | 1.00  |
| 4   | 55095264  | 55164414  | PDGFRA | amp  | 6     | 6          | 1.00  |
| 6   | 163835032 | 163999628 | QKI    | del  | 3     | 3          | 1.00  |
| 7   | 55086714  | 55324313  | EGFR   | amp  | 23    | 22         | 0.96  |
| 7   | 92234235  | 92465908  | CDK6   | amp  | 4     | 4          | 1.00  |
| 9   | 21967751  | 21995300  | CDKN2A | del  | 14    | 14         | 1.00  |
| 9   | 22002902  | 22009362  | CDKN2B | del  | 13    | 13         | 1.00  |
| 10  | 89622870  | 89731687  | PTEN   | del  | 3     | 3          | 1.00  |
| 10  | 123237848 | 123357972 | FGFR2  | amp  | 2     | 2          | 1.00  |
| 12  | 4382938   | 4414516   | CCND2  | amp  | 2     | 2          | 1.00  |
| 12  | 58141510  | 58149796  | CDK4   | amp  | 11    | 10         | 0.91  |
| 12  | 69201956  | 69239214  | MDM2   | amp  | 7     | 7          | 1.00  |
| 17  | 73314157  | 73401790  | GRB2   | amp  | 2     | 2          | 1.00  |

Note: 'Start' and 'End' are starting and ending positions of a gene, respectively. 'Type' is amplification or deletion of the gene. 'Total' is the number of samples that were found to have an alteration around that gene in our previous study. 'Identified' is the number of samples that were detected without normal samples in this study. 'Ratio' is 'Identified' divided by 'Total'.

**Table 2.** CN-altered LUAD-related genes

| Chr | Start    | End      | Name   | Type | Total | Identified | Ratio |
|-----|----------|----------|--------|------|-------|------------|-------|
| 5   | 1253262  | 1295184  | TERT   | amp  | 2     | 2          | 1.00  |
| 5   | 58264865 | 59817947 | PDE4D  | del  | 3     | 3          | 1.00  |
| 9   | 8314246  | 10612723 | PTPRD  | del  | 2     | 2          | 1.00  |
| 9   | 21967751 | 21995300 | CDKN2A | del  | 2     | 2          | 1.00  |
| 12  | 69201956 | 69239214 | MDM2   | amp  | 2     | 2          | 1.00  |
| 19  | 30302805 | 30315215 | CCNE1  | amp  | 2     | 2          | 1.00  |

Note: 'Start', 'End', 'Name', 'Type', 'Total', 'Identified' and 'Ratio' are the same as those described in Table 1.

**Table 3.** CN-altered OVC-related genes

| Chr | Start     | End       | Name    | Type | Total | Identified | Ratio |
|-----|-----------|-----------|---------|------|-------|------------|-------|
| 1   | 40361098  | 40367928  | MYCL    | amp  | 7     | 7          | 1.00  |
| 1   | 150547032 | 150552066 | MCL1    | amp  | 4     | 4          | 1.00  |
| 3   | 168801287 | 169381406 | MECOM   | amp  | 7     | 7          | 1.00  |
| 4   | 1723227   | 1746898   | TACC3   | amp  | 5     | 5          | 1.00  |
| 4   | 73939093  | 74124515  | ANKRD17 | amp  | 2     | 2          | 1.00  |
| 5   | 1253262   | 1295184   | TERT    | amp  | 4     | 4          | 1.00  |
| 6   | 19837617  | 19840915  | ID4     | amp  | 4     | 4          | 1.00  |
| 8   | 55370495  | 55373448  | SOX17   | amp  | 7     | 7          | 1.00  |
| 8   | 128747680 | 128753674 | MYC     | amp  | 16    | 16         | 1.00  |
| 10  | 89622870  | 89731687  | PTEN    | del  | 6     | 6          | 1.00  |
| 11  | 77811982  | 77850706  | ALG8    | amp  | 6     | 6          | 1.00  |
| 12  | 25357723  | 25403870  | KRAS    | amp  | 4     | 4          | 1.00  |
| 13  | 48877887  | 49056122  | RB1     | del  | 4     | 4          | 1.00  |
| 14  | 21457929  | 21465189  | METTL17 | amp  | 3     | 3          | 1.00  |
| 17  | 29421945  | 29709134  | NF1     | del  | 3     | 3          | 1.00  |
| 19  | 30302805  | 30315215  | CCNE1   | amp  | 16    | 16         | 1.00  |

Note: 'Start', 'End', 'Name', 'Type', 'Total', 'Identified' and 'Ratio' are the same as those described in Table 1.

level 3 data of the same TCGA samples, where denoised  $CN_{Wabico}$  and  $CN_{BIC-Seq2}$  served for calculating correlation coefficients. Table 4 reveals that the WGS samples corrected by means of Wabico have higher correlation values with SNP array level 3 data than those corrected by the BIC-Seq2 normalization method for

**Table 4.** The number of WGS cancer samples having greater correlation coefficients with the Wabico or BIC-Seq2 method

| Cancer | Total | Wabico | BIC-Seq2 | P-values |
|--------|-------|--------|----------|----------|
| GBM    | 37    | 30     | 7        | 0.010    |
| LUAD   | 28    | 24     | 4        | 0.023    |
| OVC    | 47    | 25     | 22       | 0.116    |

Note: 'Cancer' is a cancer type of TCGA WGS datasets. 'Total' is the number of cancer patients in the dataset. 'Wabico' is the number of patients with a greater correlation coefficient between SNP level 3 segment and denoised CN values corrected by Wabico than that between SNP array level 3 segment and denoised CN values corrected by BIC-Seq2-based expected read counts. 'BIC-Seq2' is the case opposite to 'Wabico'. 'P-values' are obtained by a paired *t*-test.

GBM, LUAD and OVC WGS datasets. Supplementary Tables S5, S6 and S7 give correlation values for the GBM, LUAD and OVC samples, respectively. We performed the paired *t*-test for the difference in correlation coefficients for samples of each cancer type. For GBM and LUAD, there were significant differences, but there was no significant difference for OVC, as shown in the last column of Table 4. Moreover, because the correlations were calculated by means of most markers in the whole genome, they were mostly affected by broad CN changes rather than by focal aberrations. Thus, this result implies that broad CN aberrations can be identified more effectively via the correction using Wabico than the correction using the BIC-Seq2-based expected read count.

In addition, for a further comparison, we applied a CN segmentation method to WGS data that are GC-corrected by Wabico and BIC-Seq2-based expected read counts, and then measured the precision, recall and F1-scores of CN segments by comparing them with CN segments in SNP array level 3 data. F1-scores of CN segments corrected by Wabico were higher than those corrected by the BIC-Seq2-based expected read count in greater numbers of samples for all three tumor datasets. Detailed results are given in Supplementary Tables S8, S9 and S10.

## 4 Discussion

We developed a new GC bias correction method. We decomposed original DOC into scaling and wavelet coefficients and fitted each coefficient by LOESS regression and kernel smoothing, respectively. After generating  $DOC_{GC}$ , we reduced the GC bias by dividing original DOC by  $DOC_{GC}$ .

We employed variable-size windows for quantifying the mapped reads as BIC-Seq2 did. It has an advantage of reducing the effect of mappability bias by taking into account only uniquely mappable positions. In the wavelet decomposition, we calculated differences and averages of two neighboring genomic regions although their actual genomic lengths could be different. When we set the windows to contain 100 uniquely mappable positions, most of window sizes were 100 bp in hg19. When we manually inspected already known alterations, the effect of variable-size windows did not seem to be substantial.

In Wabico, we used a multiresolution approach to control GC bias. At a given decomposition level,  $DOC_{GC}$  is calculated from GC bias information from the lowest level to that level. Note that the degree of uncertainty in the  $DOC_{GC}$  signal can change according to the decomposition level. As illustrated in Figure 8(c and d), deletion events in Figure 8(c) are removed in Figure 8(d). As the level increases, some false positive events can be removed although true

events might be removed as well. Thus, the choice of proper decomposition levels is important. Therefore, in this study, we set the minimal ratio of the direction of changes to the value consistent with the initial direction of changes, 50%. As we increase decomposition levels, consistency values with the initial direction of changes decrease overall (Fig. 4). When the ratios of the consistency fall below 50% at some levels, the plots of  $DOC_{GC}$  for these levels seem to be distorted and do not appear to properly reflect the GC bias embedded in raw input DOC signals. Although this is not a mathematically rigorous decomposition stopping criterion, it works practically well for both simulated and real WGS datasets.

We applied Wabico to the three WGS different tumor types. In the GBM and LUAD data, the WGS samples corrected by Wabico showed significantly higher correlation with SNP array level 3 data than those corrected by the BIC-Seq2 expected read count method while the difference between two methods was marginal in the OVC data. This different result depending on cancer type might be due to other factors in addition to the severity of GC bias. For example, we observed that in the given WGS datasets, the OVC samples are CN altered in more genomic regions than the GBM and LUAD samples. Thus, more research is required to investigate the effect of other factors such as cancer characteristics for detecting the CN alterations.

CNVkit (Talevich *et al.*, 2016) is a tool for identification of CN variations in whole-exome sequencing data and provides correction of GC bias in whole-exome sequencing data. To correct GC bias, it employs a rolling median. Those authors reported that on sample data, the rolling median and the LOESS method produced similar fits. Because our method involves the LOESS regression based on multiresolution decomposition, we compared the performances between Wabico and the GC correction method used in the CNVkit method. Wabico showed better performance for all the three tumor types. Comparison details are described in Supplementary Tables S11, S12 and S13 and Figure S8.

Wabico helps to visually inspect fluctuations of the DOC signal that can be checked by GC bias (Figs 5c, 6, 8 and 9]. Furthermore, the DOC values corrected by Wabico can serve as input to segmentation algorithms such as BIC-Seq2 and circular binary segmentation (Olshen *et al.*, 2004) for identifying the exact breakpoint of a CN alteration or for determining integer CNs of genomic regions.

## Funding

This work has been supported by a National Research Foundation of Korea (NRF) grant funded by the Korea government (NRF-2016R1A2B2013855), the Bio & Medical Technology Development Program of NRF funded by the Korean government (MSIT) (NRF-2018M3C7A1054935) and GIST Research Institute (GRI) grant funded by the GIST in 2018.

## References

- Benjamini, Y. and Speed, T.P. (2012) Summarizing and correcting the gc content bias in high-throughput sequencing. *Nucleic Acids Res.*, **40**, e72.
- Boeva, V. *et al.* (2011) Control-free calling of copy number alterations in deep-sequencing data using gc-content normalization. *Bioinformatics*, **27**, 268–269.
- Cleveland, W.S. (1979) Robust locally weighted regression and smoothing scatterplots. *J. Am. Stat. Assoc.*, **74**, 829–836.
- Coifman, R.R. and Donoho, D.L. (1995) Translation-invariant de-noising. *Wavelets Stat.*, **103**, 125–150.
- Douglas, N. *et al.* (2015) *fields: Tools for Spatial Data. R Package Version 9.0.* [www.image.ucar.edu/~nychka/Fields](http://www.image.ucar.edu/~nychka/Fields)
- Hur, Y. and Lee, H. (2011) Wavelet-based identification of dna focal genomic aberrations from single nucleotide polymorphism arrays. *BMC Bioinform.*, **12**, 146.
- Jang, H. *et al.* (2016) Identification of cancer-driver genes in focal genomic alterations from whole genome sequencing data. *Sci. Rep.*, **6**, 25582.
- Magi, A. *et al.* (2012) Read count approach for dna copy number variants detection. *Bioinformatics*, **28**, 470–478.
- Olshen, A.B. *et al.* (2004) Circular binary segmentation for the analysis of array-based dna copy number data. *Biostatistics*, **5**, 557–572.
- Ritchie, M.E. *et al.* (2015) Limma powers differential expression analyses for RNA-sequencing and microarray studies. *Nucleic Acids Res.*, **43**, e47.
- Scheinin, I. *et al.* (2014) Dna copy number analysis of fresh and formalin-fixed specimens by shallow whole-genome sequencing with identification and exclusion of problematic regions in the genome assembly. *Genome Res.*, **24**, 2022–2032.
- Talevich, E. *et al.* (2016) Cnvkit: genome-wide copy number detection and visualization from targeted dna sequencing. *PLoS Comput. Biol.*, **12**, e1004873.
- Teo, S.M. *et al.* (2012) Statistical challenges associated with detecting copy number variations with next-generation sequencing. *Bioinformatics*, **28**, 2711–2718.
- Xi, R. *et al.* (2016) Copy number analysis of whole-genome data using bic-seq2 and its application to detection of cancer susceptibility variants. *Nucleic Acids Res.*, **44**, 6274–6286.
- Xia, Y. *et al.* (2017) Pysim-sv: a package for simulating structural variation data with gc-biases. *BMC Bioinform.*, **18**, 53.